

# Autologous cell therapy with CD133+ bone marrow-derived stem cells for Asherman Syndrome: a phase 1/2 trial

Received: 3 February 2025

Accepted: 10 December 2025

Cite this article as: Santamaria, X., Pardo-Figuerez, M., González-Fernández, J. *et al.* Autologous cell therapy with CD133+ bone marrow-derived stem cells for Asherman Syndrome: a phase 1/2 trial. *Nat Commun* (2025). <https://doi.org/10.1038/s41467-025-67850-x>

Xavier Santamaria, María Pardo-Figuerez, Javier González-Fernández, Sergi Querol, Luciano Rodríguez, David Valcárcel, Carla González, Estefanía Fernandez, Diego Amorós, Michael Robles, Sofia Granados-Aparici, Sheila Zuñiga, Francisco Martínez, Diana Valbuena, Carlos Gómez, Julio Herrero, Ramon Aurell, Juan José Torrent, Felipe Vilella, Petr Volkov, Francisco Raga, Rosa Noguera, Hugh S. Taylor & Carlos Simón

We are providing an unedited version of this manuscript to give early access to its findings. Before final publication, the manuscript will undergo further editing. Please note there may be errors present which affect the content, and all legal disclaimers apply.

If this paper is publishing under a Transparent Peer Review model then Peer Review reports will publish with the final article.

## Autologous cell therapy with CD133+ bone marrow-derived stem cells for Asherman Syndrome: a phase 1/2 trial

**Formatted:** Right: 1", Top: 1", Bottom: 1", Section start: New page, Width: 8.5", Height: 11", Numbering: Continuous

Xavier Santamaria<sup>1,2#</sup>, María Pardo-Figuerez<sup>1</sup>, Javier Gonzalez-Fernandez<sup>1</sup>, Sergi Querol<sup>3</sup>, Luciano Rodríguez<sup>3</sup>, David Valcárcel<sup>4</sup>, Carla González<sup>5</sup>, Estefanía Fernandez<sup>1</sup>, Diego Amorós<sup>1</sup>, Michael Robles<sup>1</sup>, Sofia Granados-Aparici<sup>6,7,8</sup>, Sheila Zuñiga<sup>7</sup>, Francisco Martinez<sup>7</sup>, Diana Valbuena<sup>9</sup>, Carlos Gómez<sup>9</sup>, Julio Herrero<sup>2</sup>, Ramon Aurell<sup>10</sup>, Juan José Torrent<sup>11</sup>, Felipe Vilella<sup>1,7</sup>, Petr Volkov<sup>1</sup>, Francisco Raga<sup>7,12</sup>, Rosa Noguera<sup>6,7,8</sup>, Hugh S. Taylor<sup>13</sup> and Carlos Simon<sup>1,7,12,14#</sup>

<sup>1</sup>Carlos Simon Foundation, Valencia, Spain

<sup>2</sup>Department Ob/Gyn Vall d'Hebron Institut de Recerca (VHIR), Barcelona, Spain

<sup>3</sup>Department of Cell Therapies, Banc de Sang i Teixits, Barcelona Spain

<sup>4</sup>Department of Hematology, Vall Hebron Institut Oncologia (VHIO), Barcelona Spain

<sup>5</sup>Department of Vascular Radiology, Vall Hebron Institut de Recerca (VHIR), Barcelona, Spain

<sup>6</sup>Department of Pathology, Medical School, University of Valencia, Valencia, Spain

<sup>7</sup>INCLIVA Health Research Institute, Valencia, Spain

<sup>8</sup>Centro de Investigación Biomédica en Red de Cáncer, Instituto de Salud Carlos III, Madrid

<sup>9</sup>Igenomix R&D, Valencia, Spain

<sup>10</sup>Department of Human Reproduction, Clínica Quirón, Barcelona, Spain.

<sup>11</sup>Department of Obstetrics & Gynecology, Hospital Pilar, Barcelona Spain

<sup>12</sup>Department of Pediatrics Obstetrics & Gynecology, University of Valencia, Valencia, Spain

<sup>13</sup>Department of Obstetrics, Gynecology and Reproductive Sciences, Yale School of Medicine, New Haven, CT, USA

<sup>14</sup>Department of Obstetrics and Gynecology, Beth Israel Deaconess Medical Center, Harvard Medical School, Boston, MA, USA

<sup>#</sup> Correspondence: [xsantamaria@fundacioncarlossimon.com](mailto:xsantamaria@fundacioncarlossimon.com)

ARTICLE IN PRESS

**Abstract**

Autologous CD133+ bone marrow-derived stem cell (BMDSC) therapy has been designated as an Orphan Drug by the EMA and FDA for the treatment of Asherman Syndrome (AS). This phase 1/2, non-randomized, open-label, single-arm trial assessed the safety and efficacy of this novel therapy in 20 infertile women with moderate to severe AS, unresponsive to prior hysteroscopic treatments.

Primary endpoints were safety and tolerability over 15 months follow-up, including during pregnancy and after live birth. The therapy was well tolerated with a mean dosage of  $125.41 \times 10^6$  cells, with no treatment-related serious adverse events and only reversible events such as arm pain, headache, and nausea. In pregnant patients, minor obstetric complications were reflux-related cough (n=1), gestational diabetes (n=2), cervical shortening requiring pessary placement (n=2), and postpartum placenta accreta (n=1). No preterm labor occurred, and all six newborns remained free of significant adverse events. Our findings suggest that autologous CD133+ BMDSC therapy is a safe and effective treatment for AS.

Clinical trial registration (Eudra CT): 2016-003975-23

## INTRODUCTION

Asherman Syndrome (AS) is an acquired pathological condition affecting women's reproductive health, triggered by the substitution of a bona fide endometrium with intrauterine adhesions (IUAs) that cause the uterine walls to adhere to each other. Clinically, AS results in menstrual abnormalities (amenorrhea or oligomenorrhea), pelvic pain, infertility, recurrent miscarriage and abnormal placentation<sup>1</sup>.

The onset of AS is mainly caused by procedures such as postpartum curettage of the uterine cavity, after miscarriage and/or infection. These events can disrupt the endometrial niche where progenitor/stem cells may reside<sup>2</sup> causing a significant reduction in endometrial epithelial compartment and a dysfunctional pro-fibrotic, pro-inflammatory, and anti-angiogenic environment<sup>3</sup>.

Hysteroscopic adhesiolysis is the current standard treatment with limited clinical results, especially in the moderate and severe stages<sup>4–6</sup>. Advanced cell therapies have emerged as a potential therapy for AS aiming to treat with cells what cannot be treated by drugs<sup>7</sup>. Specifically, autologous CD133+ bone marrow derived stem cells (BMDSCs) were initially used to treat AS in a murine model of AS<sup>8,9</sup>. Then, a proof-of-concept trial provided preliminary evidence of the safety and therapeutic benefit of this investigational product in patients with moderate/severe AS refractory to operative hysteroscopy treatments<sup>10</sup>. As a result, autologous CD133+ BMDSCs were granted Orphan Drug designation for the treatment of AS by both the European Medicines Agency (EMA) and the U.S. Food and Drug Administration (FDA)<sup>11</sup>.

We present a 15-month follow-up study from a non-randomized, open-label, phase 1/2 trial for 20 patients experiencing clinical symptoms including infertility, due to moderate or severe AS according to the IUAs ASRM classification<sup>12</sup>, those who are refractory to operative hysteroscopy

treatments. Here, we describe the safety, effectiveness in terms of therapeutic outcomes, and biological plausibility at single cell level of autologous CD133+ BMDSC treatment.

## RESULTS

### Participant identification and baseline characteristics

This is a prospective, single-arm, open-label, non-randomized, phase 1/2 trial, in which we enrolled infertile patients with a hysteroscopic diagnosis of moderate or severe AS according to the IUAs ASRM classification<sup>12</sup>. This clinical trial involved administration of an advanced therapy medicinal product (ATMP) during the simulated secretory phase (5 days after progesterone administration), where the use of autologous CD133+ BMDSCs was approved by the Spanish Agency of Medicines and Medical Devices (AEMPS, April 20<sup>th</sup>, 2020) and the Clinical Research Ethics Committee at the Hospital Universitari Vall D'Hebron Barcelona, Spain (April 17<sup>th</sup>, 2020, IGX1-ENT-XS-16-01). Following diagnostic hysteroscopy, hematopoietic stem cells were mobilized, harvested through leukapheresis, and selected for CD133+ before intra-endometrial spiral arterioles instillation. Although the minimum accepted range of mobilized cells was at least 30 million cells with a >70% purity and >50% viability, the average of CD133+ instilled cells was  $125.41 \times 10^6$  cells with a purity of  $89.54 \pm 8.29\%$ , and a viability of  $99.7 \pm 0.27\%$ , exceeding minimum thresholds. An overview of the study design is described in **Figure 1A**.

Between September 7<sup>th</sup>, 2020 and September 19<sup>th</sup>, 2022, 24 patients were screened for eligibility, 20 were enrolled and received autologous CD133+ BMDSC therapy (**Figure 1B**). A detailed summary of clinical characteristics of participants pre- and post-AS therapy is presented in **Table 1**.

The mean age of patients was 38.3 years (IQR 37.5-40). The average number of previously attempted reparative operative hysteroscopies was 3.2 (range 1 to 11). Despite previous surgical treatments, no patient reported significant improvement of their endometrial thickness, volume, hysteroscopic scores, and none had achieved pregnancy after AS was diagnosed (**Table 1**).

### Primary endpoints

The primary endpoints of this study were to evaluate safety and tolerability of this autologous cell therapy with up to 15 months follow-up, during pregnancy and in cases of live birth. The therapy was well tolerated at doses ranging from  $37$  to  $166.1 \times 10^6$  cells (mean dosage  $125.41 \times 10^6$  cells). No serious adverse events related to the medicinal product were observed and no haemopoietic malignancies were reported. The most common adverse events after stem cell administration included arm pain, headache and nausea, which in all cases were mild and reversible. Arm pain was mostly related to catheterization and was solved with local ice administration. A detailed list of adverse events is presented in **Table 2**.

Among the pregnant patients, no serious adverse events were observed beyond common obstetric complications. One patient experienced a persistent cough attributed to gastroesophageal reflux. Two patients developed gestational diabetes, which was successfully managed through dietary interventions. Cervical shortening requiring pessary placement occurred in two cases. Additionally, one patient presented placenta accreta after delivery, requiring manual placental extraction and blood transfusion. Notably, there were no cases of preterm labor and no significant adverse events were reported in the six newborns during the first month of life.

#### Secondary endpoints

The secondary endpoints included endometrial morphometry, thickness, volume, uterine hysteroscopic scores, and endometrial function evaluated by menstruation recovery and pregnancy outcomes. Endometrial morphometry was obtained from the biopsies extracted analyzed by digital analysis of H&E-stained endometrial biopsy sections before and one month after therapy (**Supplementary Figure 1A**). After cell therapy, we observed a 62% increase in gland percentage, a 64% reduction in fiber-rich stroma, and a 73% increase in vessel percentage within the stroma. Additionally, a statistically significant decrease in gland area and gland lumen was noted (**Supplementary Figure 1A**).

Analysis on endometrial thickness showed an improvement in all patients analyzed (**Figure 2A**) from the maximal value of 4.90 mm (range 3-4.9 mm) with a mean of  $3.80 \pm 0.95$  mm pre-AS therapy to a maximal thickness post-AS therapy of 6.50 mm (range 4-6.5mm) with a mean value of  $5.29 \pm 0.77$ mm ( $p < 0.05$ ) (**Figure 2B, Table 1**). Endometrial volume as assessed by 3D

ultrasound also increased in all patients (**Figure 2A**) with a mean of  $1.26 \text{ cm}^3$  (range  $0.27\text{-}3.5 \text{ cm}^3$ ) before, versus  $2.78 \text{ cm}^3$  (range  $0.48\text{-}4.9 \text{ cm}^3$ ) after cell therapy ( $p<0.05$ ) (**Figure 2C, Table 1**).

Hysteroscopic scores according to the IUAs ASRM classification<sup>12</sup> performed before (pre-AS therapy) and approximately one month after cell therapy (post-AS therapy), revealed improvements in the endometrium and the uterine cavity for the patients (**Figure 3A**). IUAs score pre-AS therapy was  $8.0\pm3.17$ , whereas post-AS therapy was reduced to  $4.42\pm2.09$  ( $p<0.0001$ , **Figure 3B**). More specifically, 6 out of 8 severe AS cases improved to moderate stage, 1 improved to mild stage and 1 remained as severe but with a better score. From the rest of the 12 moderate AS patients, 8 improved to a mild stage and 4 improved their IUA to a moderate score.

Endometrial function post-AS therapy was assessed clinically by the recovery of menstrual function in terms of pictorial blood loss assessment, as previously reported<sup>13</sup>. We used a validated menstrual pictogram to measure total menstrual blood loss as described in methods based on the number and staining of tampons and/or menstrual pads used per menstrual period. Each score is comparable to a milliliter of blood loss. Most patients did not have their period prior to the treatment and so menstrual blood records were prospectively assessed after therapy (1-6 months), as stated per protocol. Menstrual blood loss records showed an increase from  $29.60\pm45.40 \text{ mL}$  in the first month post-therapy to  $56.66\pm107.41 \text{ mL}$  after 2 months post-therapy. Data showed then a decrease in the records, with  $27.66\pm19.79 \text{ mL}$  in the last month after treatment (M6) (**Table 3**).

As per the reproductive outcomes among the 20 treated patients, one live birth resulted from a spontaneous pregnancy post-therapy and 5 live births resulted after ARTs. In total, we performed a total of 41 single embryo transfers in 19 patients yielding an implantation rate of 31.7% per embryo transferred (13/41). Out of these transfers, as stated above, we obtained 5 live births corresponding to a 12.19% of live birth rate per transfer attempt. When analyzed per patient, the cumulative pregnancy rate was 55% (11/20), and the cumulative live birth rate was 30% (6/20) (**Table 1**). Interestingly, the patients who achieved a live birth had been diagnosed with moderate stage AS, suggesting that treatment efficacy may be influenced by disease severity. However, given the small sample size and data heterogeneity—the unequal distribution of moderate and severe cases—this observation should be considered preliminary.

The analysis of associations between pre- and post-AS therapy changes in endometrial volume, thickness, IUA scores, and morphometry revealed statistically significant differences between patients who achieved live birth (LB) and those who experienced miscarriage. Specifically, LB was significantly associated with post-AS therapy increases in endometrial volume and thickness (**Supplementary Figure 1B**). In contrast, the miscarriage group exhibited significant changes in endometrial thickness and IUA scores (**Supplementary Figure 1C**). These findings suggest that achieving an endometrial thickness of approximately  $5.46\pm0.89$  mm and an endometrial volume of around  $3.62\pm0.85$  cm<sup>3</sup> may be associated with improved live birth outcomes in this study. Although we showed a potential association between enhanced endometrial characteristics and improved reproductive outcomes, it is important to note that live birth outcomes are also influenced by embryo transfer-related factors, such as embryo quality, number of transfers, timing, etc. These elements likely interact to determine overall success and need to be taken into consideration.

Associations between obstetrical outcomes revealed that the time range to achieve a successful pregnancy was 77 to 313.7 days (75% CI) (**Supplementary Figure 1D**). Regarding dosage, no statistically significant differences were observed between pregnant and non-pregnant patients in terms of the number of CD133+ BMDSC cells administered, which ranged from 37 to  $166.1\times10^6$  cells (75% CI) (**Supplementary Figure 1E**).

As per endometrial functionality obtained (obstetrical outcomes), three out of six deliveries were performed by cesarean section and there were 3 vaginal deliveries. All deliveries were at term (range 37-38.6W). All the newborns had normal weights (mean 3399 gr; range 3040-3970 gr) and normal development at one month. None displayed any signs of infection and there were no recorded congenital abnormalities. One of the participants experienced a first-trimester miscarriage that required hysteroscopic removal of the retained products of conception.

### Exploratory endpoints

#### Single-cell RNA sequencing of the AS endometrium pre- and post-AS therapy

Previously, we published the AS endometrial cell atlas at single-cell resolution describing syndrome-associated alterations in cell types, cell-to-cell communication and gene expression profiles that supported a dysfunctional pro-fibrotic, pro-inflammatory, and anti-angiogenic

environment<sup>3</sup>. We had previously characterized the transcriptomic profile of AS (pre-AS therapy) and identified up to 18 cell types, including two unique cell types only present in AS (AS epithelium-SLPI+ and a population of smooth muscle cells). These same patients, who received CD133+ stem cell treatment during the simulated secretory phase, are now presented in the current study with both pre- and post-AS therapy endometrial biopsies (nine out of the 20 enrolled patients, **Supplementary Figure 2A**). In parallel, we also performed single cell RNA-sequencing (scRNA-seq) profiling of the CD133+ product, which revealed a heterogeneous composition consistent with mobilized progenitor cell populations (**Supplementary Figure 2B**).

For the endometrial biopsies, scRNA-seq yielded 123,250 cells (40,336 pre-AS therapy vs. 82,914 post-AS therapy, **Figure 4A, Supplementary Figure 2C**). We integrated matched pre-treatment (pre-AS therapy) and post-treatment (post-AS therapy) samples into the same dimensional reduction depiction. Overall, we observed a tendency towards an increase on the epithelial, stromal, endothelial and perivascular compartments (**Figure 4A, Supplementary Figure 2D, 2E**), a significantly reduced AS-characteristic epithelium (0.22% vs. 0.017%), and decreased macrophage populations (0.61% vs. 0.21%) (**Figure 4A, C**). Notably, we previously showed that AS-epithelial population expresses high levels of *SLP1*<sup>3</sup>. When comparing the SLPI signal in pre and post-AS therapy samples, we observed that fluorescence was markedly reduced in post-AS therapy samples, which may account for the decrease in this cell population following CD133+ BMDSC treatment (**Supplementary Figure 2F**).

We also determined the differential gene expression between pre- and post-AS therapy in different cell types related to a gene set associated to endometrial function (see Methods). The results revealed that epithelial, AS-epithelial, stromal, endothelial, and PV cells presented a higher expression of the gene set after CD133+ BMDSCs treatment, suggesting that cell treatment reactivates endometrial functionality (**Figure 4B**). Further differential gene expression evaluation between pre- and post-AS therapy in epithelial cells revealed an increase in post-AS therapy samples of *SCGB1D2* (related to functional secretory activity), *PDGFRA* and *IGF1*, associated with extracellular matrix remodeling and regeneration. We also observed the reduced expression of *S100A10* and genes related to inflammation and immune response in post-treatment epithelial cells. These gene expression differences suggest that autologous cell therapy in the AS endometrium induces the appearance of an epithelium with reduced immune activity and

inflammation and restores secretory and regenerative functions. The stromal cell cluster in the AS endometrium after autologous cell therapy exhibited the upregulated expression of genes related to angiogenesis and vascular development such as *IGFBP2* and *PTN* (**Supplementary Figure 3**).

Analysis of the endothelial compartment indicated a transcriptomic shift from a pro-inflammatory profile characterized by cell stress to a more homeostatic state (**Supplementary Figure 3**). We observed the downregulation of genes involved in leukocyte/myeloid trans-endothelial migration (*ICAM*), antigen presentation (*HLA-DRA* and *HLA-DRB5*), cell proliferation (*FOS* and *JUNB*) or heat shock proteins (*HSPH1* and *HSPA1B*). Furthermore, *IGFBP2* overexpression suggested the enhanced formation of new blood vessels, and the expression of different collagen genes (e.g., *COL1A1*, *COL3A1*) indicated ECM cell adhesion and the development of capillaries from vessel surroundings.

Cell-to-cell communication (CCC) analysis related to immune response and pro-inflammatory pathways revealed a post-AS therapy enrichment in TWEAK, CX3C, IGF and GDF (**Figure 4D**) and a reduced in strength after CD133+ BMDSC administration in RESISTIN, IL4, ICAM and LIGHT (**Figure 4D**). Within the LIGHT pathway, we observed a disruption in established CCC between CD8+ T cells and various cell types (including stroma, epithelium, endothelium, PV, and immune cells), which was accompanied by a decline in LIGHT signaling between MAIT and stromal cells (**Supplementary Figure 4A**). Pre-AS therapy samples also displayed IL4 and RESISTIN signaling pathway activation, which suggested a strong immune activity AS endometrium. Importantly, CD133+ BMDSC administration prompted the loss of these signaling pathways, contributing to the restoration of a homeostatic environment in the endometrium (**Supplementary Figure 4B, C**).

Endometrial regeneration after damage has been linked to the activity of the canonical and non-canonical WNT pathways. In this case, CD133+ BMDSC administration prompted the recovery of CCC between the stroma, epithelium, and contractile cells in the WNT signaling pathway (**Supplementary Figure 4D**).

Angiogenic pathways involving ANGPTL showed notable changes in CCC interactions following CD133+ BMDSC therapy (**Supplementary Figure 4E**). Specifically, we observed a shift toward

increased ANGPTL2-mediated interactions in the post-AS therapy group which was validated by immunofluorescence (**Supplementary Figure 4E, F**). Given that a balance between ANGPTL1 and ANGPTL2 is critical for angiogenesis and vascular regeneration regulation, the increased ANGPTL2 signaling may reflect a regenerative response induced by the therapy.

Overall, CCC data suggested that CD133+ BMDSC therapy partially restores epithelial populations to a healthier state, enhances cell functionality by reducing oxidative stress and inflammation and promotes angiogenesis.

#### **Lineage tracing differentiation of engrafted CD133+ cells**

To track grafting and differentiation of infused CD133+ BMDSCs after cell therapy, we identified unique mitochondrial DNA (mtDNA) variants present in CD133+ BMDSCs before therapy, which were subsequently detected in various differentiated endometrial cell lineages post-therapy. Mitochondrial alteration enrichment from single-cell transcriptomes (MAESTER) was utilized for this analysis to establish relatedness<sup>14</sup>. Since the MAESTER technique requires reamplification of residual cDNA from single-cell RNA sequencing libraries, we had sufficient high-quality cDNA to perform the analysis in only three patients (N7, N9, and N15). Comprehensive profiling in these three patients revealed 32, 9 and 2 shared mtDNA variants in the endometrium post-treatment, respectively, all of which were absent before the stem cell therapy. RNA-based UMAP clustering post-treatment demonstrated the presence of CD133+ mtDNA clones within diverse endometrial cell populations (**Figure 4E**), confirming the grafting and multilineage differentiation capacity of CD133+ BMDSC post-cell therapy.

#### **Single-cell RNA sequencing of endometrial epithelial organoids (EEOs) derived from endometrial biopsies pre- and post-AS therapy**

We also profiled endometrial epithelial organoids (EEOs) from pre- and post- AS therapy and controls at the single-cell level to compare this model with our *in vivo* data. We collected pre- and post-therapy endometrial samples from three AS patients and three controls (**see supplementary data 1**), generated EEOs and passaged them twice to remove stromal cell contamination (**Figure**

**5A**). Data showed a significant enhancement in organoid-forming capacity (measured as the number of EEOs generated from the same number of cells) in control and post-AS therapy EEOs compared to pre-AS therapy EEOs ( $p<0.05$ ). After passage 2, the organoid-forming capacity of cells from the three conditions displayed no significant differences, suggesting the positive selection of organoid-forming cells after 2 passages (**Figure 5A**).

scRNA-seq of progesterone-treated EEOs yielded transcriptomic profiles from 49,609 cells in total: 14,459, pre-AS therapy, 19,556, post-AS therapy and 15,594 for controls. Seven populations were identified, consistent with previously characterized AS-derived epithelial organoids<sup>3</sup>, including glandular, glandular secretory, ciliated, cycling cells (cycling org), proliferative KRT19+, proliferative EMT and KRT17+ cells (**Figure 5B**).

In terms of cell percentage, post-AS therapy EEOs showed a higher proportion of proliferative EMT and KRT9 cells than control EEOs and pre-AS therapy EEOs, which could suggest an enhanced proliferative capacity after therapy, although the trend was non-significant. Notably, the ratio glandular secretory/glandular was similar for post-AS therapy EEOs and control EEO (ratio 3.22 and 3.69, respectively), whereas the ratio remained lower for pre-AS therapy (ratio 1.03). Although the proportions of post-AS therapy do not fully mirror those of healthy controls, the shift in epithelial glandular composition after treatment may indicate a trend toward functional remodeling, including an enrichment of cells with a potentially more receptive-like profile (**Figure 5C**). These results suggest that EEOs represent a useful *in vitro* model for studying AS, demonstrating partial recovery of AS EEOs after CD133+ BMDSC therapy to a state resembling control EEOs.

## DISCUSSION

The outbreak of many clinical trials exploring the potential of stem cells to replace or supplement tissues in debilitating or life-threatening diseases is a turning point for the field. Here, we report the safety, effectiveness, and biological plausibility of the first cell therapy with an orphan drug–designated product for moderate and/or severe Asherman syndrome (AS) and atrophic endometrium. Clinical and reproductive outcomes for patients with moderate and severe AS after hysteroscopic removal of intrauterine adhesions (IUAs) remain suboptimal<sup>15</sup>, particularly in severe cases where recurrence rates range from 20% to 62.5%, often resulting in refractory AS<sup>16</sup>. Despite

exponential growth in the use of cell therapies such as mesenchymal stem cells (MSCs), cord blood cells, and bone-marrow derived stem cells (BMDSCs) in diverse medical conditions<sup>17</sup>, challenges persist due to the use of heterogeneous, poorly characterized cells in poorly phenotype patient populations. In contrast, our study utilized a specific, well-characterized, orphan drug–designated autologous CD133+ BMDSC therapy in refractory moderate and/or severe AS patients.

Our findings indicate that the primary endpoints of the therapy involving safety and tolerability of this autologous cell therapy were met. We could see that therapy was well tolerated with up to 15 months follow-up. Further, as a secondary endpoint, the AS patients after cell therapy achieved an implantation rate of 31.7% per embryo transferred (13/41) resulting in 5 live births. In addition, we recorded one spontaneous pregnancy. As per adverse events of live birth and newborns, no serious adverse events were observed beyond common obstetric complications, fulfilling the primary end points of safety and tolerability of the study.

The stem cell therapy also yielded significant improvements in endometrial tissue reconstruction, endometrial thickness and volume, and IUA scores. These structural enhancements translated into functional benefits, including restored menstrual function and improved reproductive outcomes. Importantly, these observations suggest that targeted cellular therapies can address the underlying pathology of AS.

The integration of scRNA-seq into this Phase 1/2 clinical trial allowed for an unprecedented granular analysis of the therapy's impact at the molecular level. Transcriptomic comparisons of endometrial cells pre- and post-AS therapy revealed the expansion of key endometrial populations, including epithelial, ciliated epithelial, endothelial, and cycling cells, as well as a reduction in pro-inflammatory macrophage population, suggesting a shift away from active inflammation toward immune resolution and tissue remodeling. This dynamic is similar to processes described in successful tissue repair across organ systems, where a timely reduction of pro-inflammatory macrophages, coupled with increased vascular support and stromal cell activation, marks a transition toward functional healing<sup>18</sup>.

The therapy also demonstrates a post-treatment increase in perivascular cells (putative pericytes), and modulated gene expression pathways central to tissue repair and regeneration. Endometrial pericytes contribute to angiogenesis, and tissue regeneration through interactions with endothelial and epithelial cells and may exhibit mesenchymal stem cell-like properties that support repair<sup>19</sup>. Moreover, upregulated genes associated with angiogenesis and migration (*IGFBP2*, *PTN*, *SPARCL1*)<sup>20</sup>, epithelial development and proliferation (*IGF1*)<sup>21</sup>, and extracellular matrix (ECM) remodeling (*PDGFRα*)<sup>22</sup> were observed. Signaling pathways associated with immune response and inflammation (CCL, CXCL, LIGHT, TNF, RESISTIN), were reduced after therapy, as well as the fibrosis-related pathway ITGB2. The therapy also restored stromal-endothelial communication through a shift in ANGPTL1/ANGPTL2 balance, and reversed fibrosis-associated signaling via the NRG<sup>23</sup> and WNT pathways<sup>24</sup>. These shifts collectively promoted an anti-inflammatory tissue environment, with reductions in immune and chronic inflammation-related genes (e.g., *MIF*, *IL6ST*, *DEFB1*, *S100A10*). As for the two AS unique cell types, AS-epithelium decreased in abundance post-therapy, however, the remaining cells were enriched in a gene set associated with endometrial function. Similarly, SMC populations displayed reduced cellular stress response (decreased expression of *S100A6*). Additionally, the use of mitochondrial variant tracking using MAESTER demonstrated grafting and clonal contribution of CD133+ BMDSCs to endometrial repair, primarily through stromal and vascular cells, consistent with prior evidence of CD133+ cells' regenerative potential in ischemic and fibrotic tissues<sup>25</sup>.

Lastly, our study also used endometrial epithelial organoids (EEO) to replicate *in vivo* findings<sup>3</sup>. Post-AS therapy, a higher formation rate of EEOs was observed, and single-cell analyses confirmed that post-treatment AS-derived EEOs resembled their control counterparts, providing an innovative platform to further investigate AS pathology and regenerative mechanisms.

While this study provides compelling evidence for the efficacy of CD133+ BMDSCs in treating moderate and severe AS, it is not without limitations. The absence of a randomized control group necessitates reliance on strong biological plausibility and a sufficiently long follow-up period to draw meaningful comparisons with other cell therapies. Nevertheless, the strengths of this study lie in its rigorous methodology, careful patient selection and classification, the use of a designated orphan drug, and oversight by an independent regulatory agency.

In conclusion, autologous CD133+ BMDSC therapy demonstrated significant histological and clinical improvements in patients with moderate and severe AS, with benefits persisting for at least 15 months post-treatment and no serious adverse events reported. These findings support the considerable potential of this orphan drug—designated therapy as a viable treatment strategy for this challenging and previously incurable condition.

## METHODS

### Study design and patients

This research complies with all relevant ethical regulations. The trial was registered at the European Union Clinical Trials Register (EU-CTR, EudraCT: 2016-003975-23; Registration date: April 1<sup>st</sup>, 2020; <https://www.clinicaltrialsregister.eu/ctr-search/trial/2016-003975-23/ES>), and the Spanish Clinical Studies Registry (REec, <https://reec.aemps.es/reec/estudio/2016-003975-23>). The investigational medical product (IMP) autologous CD133+ Bone Marrow Derived Stem Cells (BMDSC) was designated as an Orphan Drug (OD) by the EMA on April 20<sup>th</sup>, 2017 (EMA/OD/313/16)<sup>11</sup> and by the FDA on February 1<sup>st</sup>, 2019 (#DRU-2017-6131). For the design of this clinical trial, scientific advice and protocol assistance were obtained from the AEMPS (February 10<sup>th</sup>, 2017) and the EMA (September 1<sup>st</sup>, 2017), respectively. The clinical research ethics committee at Vall d'Hebron Hospital approved this research in March 2020.

Out of 24 eligible patients, we enrolled 20 patients that met inclusion criteria and provided written informed consent. Patients were referred by clinics worldwide based on their refractoriness to previous operative hysteroscopy treatments and provided written consent. The first and last patient inclusions took place on Sept 9<sup>th</sup>, 2020 and Sept 19<sup>th</sup>, 2022, respectively. A detailed summary of clinical characteristics of participants pre- and post-treatment is presented in **Table 1**.

### Study Outcomes

The primary endpoints of the trial were safety and tolerability of the autologous CD133+ BMDSC therapy by identifying the incidence, prevalence, and frequency of adverse events occurring:

1. During the study period up to 15 months post-treatment.
2. In the event of a term pregnancy
3. In a case of live birth

Secondary endpoints were the efficacy of the therapy in achieving an improvement in morphological and clinical features such as endometrial histology through digital image analysis, endometrial thickness and volume by 2D and 3D vaginal ultrasound, hysteroscopic grading scores (IUAs), menstrual function recorded monthly based on the duration (days), volume (pads/day) and frequency (days) of menstrual bleeding with the Pictorial Blood Assessment Chart<sup>13</sup>, and reproductive outcomes after treatment measured by pregnancy, miscarriage, ongoing and live birth rates. The interim results of the trial were supervised by an independent Data Monitoring Committee (DMC) with special focus on the safety data. Exploratory endpoints included the study of endometrial biopsies before and after stem cell treatment to compare differences in endometrial structure and tissue regeneration mechanisms, as the case of single cell RNA sequencing.

### Procedures

Patients were managed as previously described<sup>10</sup> with hormonal replacement therapy (HRT) to establish an endometrium with functional equivalence to the proliferative (estrogen dominant) and secretory (progesterone dominant) phases of a normal menstrual cycle before and after stem cell therapy. This was necessary as study patients experienced a lack of regular menstruation or negligible blood loss at menses. During the simulated “secretory phase” (5 days after progesterone administration) pre-treatment and post-treatment endometrial status was monitored by histological digital image analysis, 2D/3D ultrasound (Samsung, South Korea) and hysteroscopic assessment according to ASRM classification of IUAs<sup>12</sup> using a 5mm Betocchi hysteroscope (Karl-Storz, Germany). Hysteroscopic diagnostic evaluation was used to grade the severity of AS; however, no operative hysteroscopy was performed. In the four patients for whom images were unavailable, ASRM scoring was verified through direct visualization by both surgeons (X.S. and J.T) during hysteroscopy, with detailed operative notes recorded. Although this represents an unavoidable limitation, we sought to minimize potential bias by applying predefined scoring criteria and maintaining consistent documentation practices.

Endometrial biopsies were performed under hysteroscopic vision from the posterior wall of the uterus at least 1 cm away from any visually identified IUA using a semi-rigid double-action biopsy and grasping forceps (Karl-Storz, Germany). Then endometrial specimens were processed for histology, ERA<sup>26</sup> and EMMA<sup>27</sup> to assess endometrial structure, receptivity and microbiome to rule out the existence of dysbiosis, respectively. Single cell RNA seq of biopsies and endometrial organoids were also derived from these endometrial biopsies.

Eligible patients were assessed by the hematology department at Vall Hebron (Barcelona, Spain). Requirements for participation in the study included a patient age of 18–44 years old, a BMI of 18–30, normal liver, heart, and kidney function, the absence of pregnancy, HIV, Hepatitis B or C, syphilis or any psychiatric pathology, and a willingness to complete the study.

BMDSC mobilization was performed using granulocyte-CSF (G-CSF) injection at 10 mcgr/kg for 5 days. CD133+ BMDSCs were collected through peripheral blood apheresis and subsequently isolated. Patients were excluded if they did not reach the minimal requirements for mobilized cells of at least 30 million cells, a purity above 70% and a viability >50%, presented an unstable medical condition, or refused a central venous catheter when required. Isolation of mononuclear cells was then performed by apheresis through peripheral venous access using the CobeSpectra separator (Terumo BCT, Lakewood, CO, USA) according to the manufacturer instructions. Subsequently CD133+ cell selection and isolation were performed using the cell sorter CliniMACS Pro (Miltenyi Biotec GmbH, Bergisch Gladbach, Germany). A mean of 267 minutes and 2.83 volemias in the apheresis were required to obtain a product with an average viability of  $99.7\pm0.27\%$  and a mean purity of  $89.54\pm8.29\%$ . The minimum of CD133+ cells to be obtained by selection was 30 million cells that were diluted into 15–30 cc of saline solution and transported in a sterile bag with a syringe to the interventional Radiology Department at Vall Hebron Hospital for delivery.

Finally, isolated CD133+ BMDSCs were delivered into the spiral arterioles of the patient using a minimal invasive radiology intervention through the left brachial artery, using the Seldinger technique<sup>28</sup>. The method consisted of placing a 4F introducer into the artery and catheterizing using a 2-curve Cobra angiographic catheter and a 0.035" Terumo guide wire. Through the Cobra catheter, a 2.5F microcatheter with a 0.014" guide wire was inserted and used to catheterize both uterine arteries up to the most distal level allowed by the microcatheter. The procedure was carried

out under procedural sedation. Once the catheter was stabilized and its position verified, approximately 15–20 mL containing a mean CD133+ cell dose of  $122 \times 10^6 \pm 48 \times 10^6$  cells (range  $42–200 \times 10^6$  cells) were administered.

All the diagnostic procedures (2D/3D ultrasound, diagnostic hysteroscopy and endometrial biopsies) before and one month after autologous CD133+ BMDSC administration in an outpatient setting were performed by the same surgeon (X.S.). In the four patients for whom IUAs images were unavailable, ASRM scoring was verified through direct visualization by both surgeons (X.S. and J.T) during hysteroscopy. Afterwards, patients were invited to undergo single embryo transfer (SET). All safety and effectiveness outcomes were recorded during the 15 months following treatment.

#### **Pictorial Blood Assessment Chart (PBAC)**

Endometrial function after cell therapy was assessed clinically by the recovery of menstrual function in terms of blood loss with a validated menstrual pictogram<sup>7</sup>. This method uses a score based on the number and staining of tampons and/or menstrual pads used per menstrual period. Each score number is comparable to a milliliter of blood loss. Menstrual pictograms were provided after the hysteroscopy following stem cell therapy, and the patient was requested to monitor menstrual cycles for six months if any menstrual cycles occurred (See Table 3).

#### **Immunohistochemistry**

Endometrial samples were fixed with 4% paraformaldehyde overnight and embedded in paraffin for hematoxylin and eosin (H&E) staining or immunofluorescence. For immunofluorescence, 10  $\mu$ m-thick paraffin sections were deparaffinized in xylene and rehydrated through a graded ethanol series. Antigen retrieval was performed by heating the slides in 10 mM sodium citrate buffer (pH 8–9) at 95–100 °C for 20 minutes, followed by cooling at room temperature for 20 minutes. Sections were then permeabilized with 0.1% Triton X-100 in PBS for 10 minutes and blocked for 1 hour at room temperature in PBS containing 3% BSA and 0.1% Tween-20. Samples were incubated overnight at 4 °C with goat anti-ANGPTL2 primary antibody (R&D Systems, Cat# AF623) or goat anti-SLPI (R&D Systems Cat #AF1274), both diluted 1:100 in blocking buffer.

After washing with PBS, sections were incubated for 1 hour at room temperature in the dark with donkey anti-goat Alexa Fluor 488-conjugated secondary antibody (Invitrogen, 1:400). Nuclei were counterstained with DAPI (1  $\mu$ g/mL) for 5 minutes. Slides were mounted with antifade mounting medium and imaged using a Confocal fluorescence microscope Stellaris 5.

#### Digital image analysis

Endometrial biopsy sections stained with hematoxylin and eosin (H&E) were digitized with a VENTANA iScan HT slide scanner (Roche) at 20X and analyzed in QuPath<sup>29</sup>. Samples selected had intact glands and extracellular matrix (ECM), excluding regions with necrosis or hemorrhage. Gland sections from 13 patients (pre- and post-treatment) were carefully segmented using the brush and wand QuPath annotation tools and luminal epithelium was excluded to obtain a specific annotation for the gland epithelium.

Epithelial cell nuclei from the gland were then detected using StarDist, a deep-learning extension script for star-convex nuclear detection based on pre-trained datasets of H&E images (<http://github.com/qupath/qupath-extension-stardist>). Morphometric data on lumen, gland, and gland epithelium were gathered, calculating lumen percentage within glands and epithelial cell density. Stromal areas were using StarDist and ECM-related features (collagen, ground substance, and vessels) such as ingurgitated vessels and small diffuse hemorrhagic area included) were obtained by training a pixel classification-based Artificial Neural Network with full resolution (0.25  $\mu$ m/px) in QuPath. The resulting classifier corresponding to each ECM component was then applied to all samples and a percentage relative to the stroma area was obtained. Percentage of hematoxylin-stained cell nuclei was obtained by subtracting the area occupied by the ECM components to the stroma annotation. Cases with the existence of ECM underlying the uterine lumen lining epithelium with evidenced stroma decidualization were qualitatively evaluated by an expert pathologist.

#### Processing and dissociation of endometrial biopsies for single cell analysis

A two-stage dissociation protocol separated endometrial biopsies into stromal fibroblasts and epithelial-enriched single-cell suspensions. Before dissociation, tissue was rinsed with PBS in a petri dish to remove blood and mucus, and excess PBS was removed after rinsing. The tissue was

then minced into small pieces and dissociated with 3 mL collagenase mix (Collagenase V, Sigma, USA), RPMI+10% fetal bovine serum, and DNaseI (Sigma, USA) at 37°C under continuous shaking at 175 rpm for 25 min in a 15 mL Falcon tube in a horizontal position. This primary enzymatic step mostly dissociates stromal fibroblasts into single cells while leaving epithelial glands and lumen mostly undigested. The contents were transferred to a 50 mL tube in RPMI media and filtered with a 100 µm cell strainer. The tissue remaining on the filter was used for the epithelial enrichment cell isolation by resuspending and incubating in 10 mL Trypsin mix (Trypsin -EDTA (0.25%) phenol and DNaseI) for 10 min. The resulting two contents were transferred to 50 mL tubes with 20 mL RPMI, filtered with a 100 µm cell strainer, centrifuged, and then resuspended in 1 mL RPMI. Dead cells were removed using the MACS dead cell removal kit (Miltenyi Biotec, Germany). Live-cell suspensions were loaded into a Chromium Next GEM Chip G (10X Genomics, USA) to obtain cDNA from individual cells.

#### **10x Genomics Chromium library preparation and sequencing**

Cell suspension was loaded into a Chromium Next GEM Chip G (10x Genomics) and run in a Chromium Controller (10x Genomics). cDNA synthesis and amplification were performed using the Single Cell 3' Reagent Kit v3.1 (10x Genomics). 25% of the resulting cDNA was used for enzymatic fragmentation, end repair, A-tailing, adapter ligation, and amplification (with an expected yield of 0.1 ng/µl and a peak size between 200 and 9000 bp as determined in a TapeStation using HSD1000 assay reagents), serving as a quality control. Libraries were then quantified in a TapeStation using HSD1000 assay reagents.

10x-Genomics v3 libraries were prepared as per the manufacturer's instructions. Libraries were sequenced, aiming at a minimum coverage of 50,000 raw reads per cell, on an Illumina NovaSeq 6000 S2v1.5 300 cycles at a mean 40x coverage (paired-end; read 1: 26 cycles; i7 index: 8 cycles, i5 index: 0 cycles; read 2: 98 cycles)

#### **Alignment and quantification of 10X scRNA-seq data**

scRNA-seq data was processed using *Cell Ranger* v3.1.0 and *Seurat* v4. These versions were maintained to ensure consistency with a previously analyzed dataset and to enable direct comparability<sup>3</sup>. While newer versions include improvements in cell calling, UMI correction,

doublet detection, and annotation, we applied the same pipeline and stringent quality controls across all samples to minimize technical variability. Core *Seurat* steps—normalization, dimensionality reduction, clustering, and visualization—also improved across versions. Nevertheless, we consider our biological interpretations robust, while acknowledging possible limitations in sensitivity and cross-study compatibility with newer software releases.

Raw reads were demultiplexed using the *mkfastq* wrapper command for *bcl2fastq* (Illumina). Libraries were aligned to the GRCh38-3.0.0 reference genome (based on GRCh38.p12, NCBI: GCA\_000001405.27), as provided by 10x Genomics. Gene expression count matrices were generated per sample using the count pipeline with default parameters. This pipeline includes read alignment using the STAR aligner, UMI counting, barcode calling, and filtering of empty droplets. The filtering step relies on a Good-Turing smoothing model of background gene expression to distinguish low-RNA-content cells from ambient RNA.

#### **Quality control filtering of cells and doublet detection**

Low-quality cells were filtered out based on quality control metrics. Specifically, cells with a low number of detected genes or a high proportion of mitochondrial reads were excluded. All quality control procedures and downstream analyses were performed using R (v4.1).

Doublet detection was performed with two methods: *DoubletFinder* (v2.0.3) and *scds* (v1.6.0) packages. The expected doublet formation rate was fixed for each sample according to the cell count recovery given per sample by *Cell Ranger*. The hybrid approach from the *scds* package was used to avoid removing false-positive doublets. Cells marked as doublets by both algorithms were removed from the samples.

#### **Integration of scRNA-seq data across different conditions and cell clustering**

Individual samples were aggregated, processed, and integrated with functions from the *Seurat* (v4.0.1) package. First, sample-to-sample aggregation for each condition dataset was performed with the *merge* function. Next, each aggregated dataset (pre-AS and post-AS therapy) was processed with the *SCTransform*. The *SCTransform* pipeline integrates different study conditions by applying a regularized negative binomial regression to allow the detection of condition-to-condition shared cell identities and the performance of differential expression analysis.

Mitochondrial ratios and cell cycle phase were regressed out from integrated datasets. The 3000 most variable genes present in combined datasets using the *SelectIntegrationFeatures* function were used. *PrepSCTIntegration* and *FindIntegrationAnchors* were applied to identify the anchoring vectors across datasets and integration steps performed with *IntegrateData* (normalization method set to SCT). In the dimensional reduction step, the first 30 dimensions of PCA and UMAP were used to visualize cell clusters on the nearest-neighbor graphs. The *clustree* (0.4.4) package was used to evaluate the optimal resolution number in the *FindCluster* function; multiple clusters with a range of resolution from 0.5 to 3 were generated, with increased steps of 0.1. A manual review of the generated UMAPs and *clustree* output determined an optimal resolution of 0.8 to label the different clusters. The integration step was validated by evaluating the conservation of canonical markers across pre- and post-conditions.

#### **Annotation of cell types in scRNA-seq datasets**

Cell type identification was conducted by examining the differentially expressed genes of each cluster in comparison to the others. The Wilcoxon Rank Sum test was used, and the p-values were adjusted using the false discovery rate (FDR) method. Cluster cell identity was evaluated by comparison of cluster marker genes that were compared to annotated major cell types reported in published endometrial atlases<sup>10,24</sup>.

#### **Analysis of significant changes in cell population sizes**

Cell ratio analysis across different experimental groups was performed using a pseudobulk strategy. A count matrix of the different cell types detected per sample was created, and the *edgeR* (v3.34.0) package was used to compute a differential abundance (DA) test across cell types. The FDR p-value adjusting method was applied.

#### **Cell-to-cell communication network analysis**

To study the possible signaling interactions between cells, total interaction probabilities and communication information flows were determined with the *CellChat* (v1.1.3) package<sup>23</sup>. The first measure indicates the probability of communication between two cell types; the total probability of interaction is split into two parts: the probability of interaction between the sender and receiver cell, considering the number of interactions (ligand-receptor or L-R pairs expressed) and the level

of expression (strength of the interaction). A database of 229 families of signaling pathways was used to obtain information regarding interactions; this curated list of molecules considers the known structure of L-R pairs, including multimeric complexes, soluble agonists and antagonists, stimulators, and inhibitory co-receptors. The second measure, the communication information flow, assesses the amount of information exchanged between several cells through various interactions. A higher value of communication information flow between cell populations indicates a more complex communication network. The *population.size* argument in the *computeCommunProb* function was used to correct the communication weight of each cell population. The cell-to-cell communication (CCC) networks were filtered to exclude those with fewer than ten cells to achieve robust results. The *rankNet* function with a significance threshold of 0.05 was used to test for network differences between AS endometrial samples pre- and post-treatment with CD133+ BMDSCs. These comparisons included only common cell types, excluding cycling cells from the analysis. Significantly altered signaling pathways between groups are highlighted in the bar graphs of the flow of information. To explore these plots further, interaction probability scatter plots can be used to identify the receiving and sending cells. The contribution of each L-R pair to a pathway is also shown in interaction probability plots.

#### MAESTER library preparation, sequencing and analysis

The methodology was applied as previously described<sup>14</sup>. Briefly, MAESTER consists of two PCRs, whereby we would include 10x Genomics 3' v3 cDNA from where the CB and UMI of the transcripts would be retained. In the first PCR, twelve primers were used to tile across the whole mitochondrial transcriptome at 1 $\mu$ M each together with a specific barcode GoT-P5-i5-BCXX for each sample<sup>14</sup>. The mixture was as follows: 20  $\mu$ L of KAPA HiFi Hotstart ReadyMix (Thermofisher Scientific), 16  $\mu$ L of cDNA product, (diluted to achieve at least 1 ng/ $\mu$ L) along with 3  $\mu$ L of primer mix 10  $\mu$ M and 1  $\mu$ L of Got-P5-i5-BCXX (10  $\mu$ M). The PCR was set to initial denaturation at 95 °C for 3 min followed by 10 cycles of 98 °C for 20 s, 65 °C for 15 s and 72 °C for 3 min, with a final extension at 72 °C for 5 min. After amplification, each individual primer generated 12 reactions, and so these were pooled together at a ratio of: mix 1: 32  $\mu$ L; mix 2: 40  $\mu$ L; mix 3: 40  $\mu$ L; mix 4: 40  $\mu$ L; mix 5: 40  $\mu$ L; mix 6: 40  $\mu$ L; mix 7: 40  $\mu$ L; mix 8: 40  $\mu$ L; mix 9: 8  $\mu$ L; mix 10: 8  $\mu$ L; mix 11: 8  $\mu$ L and mix 12: 16  $\mu$ L.

The pooled products were purified with 1× AMPure XP beads (Beckman Coulter, USA) as per protocol instructions. After AMPure XP purification, the pooled PCR1 product was eluted in 20  $\mu$ L H<sub>2</sub>O RNase free. Thereafter, the PCR2 was performed by adding 18  $\mu$ L of the purified product from PCR1, with 2  $\mu$ L of a 5 $\mu$ M primer mix (P5-generic + GoT-P7-i7-BCXX)<sup>14</sup> and 20  $\mu$ L KAPA HiFi Hotstart ReadyMix (Thermo Fisher Scientific).

The parameters used for PCR2 were an initial denaturation at 95 °C for 3 min; six cycles of 98 °C for 20 s, 60 °C for 30 s and 72 °C for 3 min, followed by a final extension at 72 °C for 5 min. The resultant PCR was purified with 0.8X AMPure XP beads. The DNA was eluted in 20  $\mu$ L TE, quantified and sequenced accordingly. The libraries contained 0.6–50 ng/ $\mu$ L with sizes ranging from 300 to 1,500bp and were sequenced on the Illumina Nova Seq X 10B sequencing (paired-end; read 1: 28 cycles; read 2: 256 cycles, 2 x 8-bp index barcodes).

Raw sequencing data was pre-processed according to the pipeline previously described<sup>14</sup>, up to the generation of BAM files containing mitochondrial reads from individual cells in the respective scRNA-Seq samples. An additional preprocessing step was implemented to trim 50 nucleotides from the 3' ends and remove poly-A tails, using *Fastp* v0.23.4<sup>30</sup>. Then, BAM files were split by cell barcodes, and each subset was processed independently. Duplicated reads were removed using *fgbio* v2.1.0 (fulcrumgenomics/fgbio: 2.4.0 (2.4.0)). To exclude low-quality cells, the total number of covered bases per cell was calculated using *samtools* v1.19.2<sup>31</sup> and *bedtools* v2.31.1<sup>32</sup>. Only cells with coverage exceeding the overall median minus one standard deviation were retained for downstream analyses. Variant calling was performed with *LoFreq* v2.1.5<sup>33</sup> following base recalibration, which was conducted using the *GATK* toolkit v4.5.0.0<sup>34</sup> (DePristo, 2011) and *LoFreq*. The resulting VCF files were normalized using *bcftools* v1.18<sup>31</sup> and filtered. Selected variants included those detected in the CD133 population of the CD133 samples and shared with S2/E2 samples while excluding variants identified in S1/E1 samples. Additionally, variants were retained only if they exhibited a variant allele frequency exceeding 10% per cell and were detected in at least five cells, but excluded if present in  $\geq$ 90% of total cells. Filtered variants were manually reviewed using *IGV* v2.12.3<sup>35</sup>. Variants with more than 10 reads in S1/E1 were discarded. The final set of variants was added to the metadata of the scRNA-seq objects using the *Seurat* (v5.1.0) package<sup>36</sup> in R v4.2.2.

#### Differential expression and gene signature score

The *FindMarkers* function from the *Seurat* package was used to perform differential expression analysis across the treatment stages and the different cell types reported in the dataset. The Wilcoxon Rank Sum test was used, and the p-values were corrected using the FDR method. Genes with FDR values under 0.05 were considered significant. Gene set signature scoring was performed using *escape* (v1.6.0) package<sup>37</sup> and *UCell* package to study menstrual cycle function in the secretory phase between treatment groups. The *AddModuleScore* function from *UCell* package was used to compute the score for each cell present in the dataset. Finally, the score differences between treatment stages in the endothelium, epithelium, AS epithelium, perivascular (PV), and stromal cell fractions were evaluated. The *getSignificance* function was used to perform statistical testing using a Wilcoxon test; p-values were corrected using the FDR method. The following gene set related to menstrual cycle function in the secretory phase was used<sup>38</sup>: *SCGB1D2*, *MT1F*, *MT1X*, *MT1E*, *MT1G*, *CXCL14*, *WNT5A*, *SFRP1*, *ZFYVE21*, *CILP*, *SLF2*, *MATN2*, and *S100A4*.

#### Organoid culture from endometrial biopsies

Organoids were generated from AS patients' endometrium pre- and post-treatment and from healthy control endometrium. After enzymatic dissociation of the endometrial biopsies, epithelial and stromal cells were obtained and total cell numbers were counted. After centrifugation at 300 g, the pellet was resuspended in 70% Matrigel (Corning, 356231) and 30% DMEM/F12 (Thermo Fisher Scientific, 11330032) and supplemented with the ROCK inhibitor Y-27632 (1/500). The suspension was cultured in 20- $\mu$ L droplets containing 25,000 cells, deposited in prewarmed 48-well plates, and allowed to form a gel at 37°C and 5% CO<sub>2</sub> before adding culture medium. Organoid culture medium was prepared as previously described<sup>39,40</sup>. Matrigel droplets were cultured for 14-16 days in the first passage (P0) with medium changes every two days. Organoids were then grown for seven days before the following passage, with media changes every two days.

Organoids were recovered for passaging by liquifying the Matrigel droplets with ice-cold DMEM/F12 (without any growth factors, serum, or enzymes), followed by repeated pipetting to ensure maximum recovery. Organoids were then dissociated by incubation with TrypLE supplemented with Y-27632 (1/1000) and mechanically triturated. The resulting cell suspension was centrifuged at 300 g, and the pellets were resuspended in 70% Matrigel and 30% DMEM/F12

supplemented with Y-27632 and placed as droplets in 48-well plates. Two passages were performed to remove the contaminating stromal cells from the epithelial organoids. After seven days of P2 culture, organoids were dissociated for single-cell transcriptomic analysis following the same protocol described for passaging but with an additional cell counting step for the single-cell transcriptomics protocol as per manufacturer's instructions (10x Genomics).

#### **Organoid counting**

Multiple microscopy images (Thermo Fisher, EVOS M5000) were taken to count organoids present in each Matrigel droplet. Images were taken by dividing each drop into two depth sections and each section into four regions. Two images were counted diagonally from each section, and the mean from these images was calculated. This mean was multiplied by the number of divisions of each section (4) and the number of sections (2) to infer the total organoid number per drop. For each condition, two experimental replicates were measured. For organoid counting we conducted a two-way analysis of variance (ANOVA) followed by a Tukey's HSD post-hoc tests to assess pairwise comparisons between the between Control, CD133+ BMDSC pre-treatment and post-treatment AS EEOs per passage.

#### **Organoids scRNA-seq**

Single-cell RNA-seq data from organoids were aggregated, processed, and integrated using a similar approach to that described for the patient-derived samples. Briefly, integration across pre-treatment, post-treatment, and control datasets was performed using the *SCTransform* function. Dimensionality reduction was conducted based on the 750 most highly variable genes using the first 30 principal components, and cell clusters were visualized using UMAP on the nearest-neighbor graph. Finally, major cell types were identified and annotated by analyzing differentially expressed genes in each cluster, using previously described cell-type-specific marker genes<sup>10,24</sup>.

## Statistical Analysis

### Statistical analysis of clinical design

The study sample size was estimated based on the hypothesis that autologous CD133+ BMDSCs instillation in the uterine arteries improves endometrial function in terms of reproductive outcomes, specifically live birth (LB) rate. It was designed as a paired cohort study “before and after”, consisting of the same patient undergoing embryo transfer after treatment. Our hypothesis was that improvement would involve a transition from 0% prior to stem cell treatment to 28% LB rate after treatment ( $\alpha$  0.05, power=80%) which is the average LB rate reported in the context of assisted reproduction treatments by the European IVF-Monitoring Consortium<sup>41</sup>. Based on these assumptions, it was estimated that 18 patients would be required for the protocol study. Additionally, a 20% loss to follow-up was anticipated, resulting in a required total of 20 patients. The final analysis was conducted after all patients completed a 15-month follow-up after treatment. However, since the actual drop-out rate was much lower than expected (only 5%), we successfully completed 19 per protocol patients out of 20 recruited, surpassing our pre-specified target of 18 per protocol patients. Given that recruiting patients with this rare condition was challenging, and upon consultation and agreement with our Ethics Committee, we concluded recruitment once the necessary number of patients had been successfully treated and completed follow-up.

### Statistical analysis of clinical outcomes

For the secondary endpoints, a convenience sample was studied. Endometrial volume, thickness, IUA score from Figure 2, 3 and Supplementary Figure 1B, C was presented as mean $\pm$ standard deviation. Statistical significance between endometrial volume and thickness was evaluated using a parametric paired t-test. Normality assumption was confirmed by applying the Shapiro–Wilk test to assess the distribution of differences between pre and post treatment for each parameter. For the IUA score, non-parametric Wilcoxon signed-rank test was applied.

Data from digital analyses presented in Supplementary Figure 1A is presented as mean $\pm$ standard error of the mean (S.E.M). Statistical significance between general characteristics of gland and stroma in paired samples grouped based on reproductive outcome was evaluated using a parametric paired t-test whereas differences between specific characteristics of gland and stroma were

assessed using a Wilcoxon rank sum test. Statistical significance within pre- and post-AS therapy between these groups was evaluated using non-parametrical Kruskal Wallis with Dunn's test for multiple comparisons.

Statistical significance was considered when the p-value was less than 0.05 and was indicated as follows:  $p < 0.05$  (\*),  $p < 0.01$  (\*\*),  $p < 0.005$  (\*\*\*), and  $p < 0.0001$  (\*\*\*\*). Data was analyzed and represented using GraphPad Prism 8.0.1 and 10.2.0 software.

#### **Statistical analysis for single cell data of *in vivo* biopsies**

Statistical analyses were performed in software R (v4.1 and v4.2, <https://www.r-project.org>). Data from Figure 4B, displaying boxplots of gene signature enrichment scores (*UCellScore*), were statistically tested using the Wilcoxon test implemented via the *getSignificance* function from the *escape* (v1.6.0) package. P-values were adjusted using the FDR correction method.

Data from Figure 4C, showing cell type ratios boxplots, were analyzed using a negative binomial generalized linear model (NB-GLM) implemented in the *edgeR* (v3.34.0) package. Statistical significance was defined as  $\text{FDR} < 0.05$  (\*\*), and  $\text{FDR} < 0.1$  (\*).

For the data shown in Figure 4D, we conducted a differential CCC analysis between pre-treatment (Pre-AS therapy) and post-treatment (Post-AS therapy) samples using the *rankNet* function from the *CellChat* (v1.1.3) package. Statistical significance was assessed with a Wilcoxon test, applying a significance threshold of 0.001 and a p-value cutoff of 0.01. P-values were adjusted for multiple testing using the FDR correction method.

Data from Supplementary Figure 3, displaying dot plots of the differential expression between Pre-AS therapy and Post-AS therapy across different cell types, were statistically tested using the Wilcoxon test implemented via the *findMarkers* function from the *Seurat* (v4.0.1) package, with p-values corrected for multiple comparisons using the FDR method.

Supplementary Figure 4, showing cellular communication through chord plots and bar plots, was generated using the *netVisual\_aggregate* and *netAnalysis\_contribution* functions from the *CellChat* (v1.1.3) package, respectively. A p-value threshold of 0.05 was applied to define significant interactions and contributions.

### Statistical analysis for organoids

For organoid counting we conducted a two-way analysis of variance (ANOVA) followed by a Tukey's HSD post-hoc tests to assess pairwise comparisons between the groups. Data was analyzed and represented using GraphPad Prism 8.0.1 and 10.2.0 software.

### Data availability

All raw data generated from this paper is presented in the source data file. The raw single-cell RNA-sequencing data generated for this manuscript has been uploaded to Gene Expression Omnibus under accession numbers GSE311899 and GSE311897. The GSE311899 dataset contains the *in vivo* endometrial samples pre- and post-AS therapy from AS patients, and the GSE311897 dataset includes all EEO samples. The uploaded data include (1) RDS files containing the aggregated count matrices and metadata of each cell studied and (2) per-sample count matrices. The raw sequences are not publicly available due to privacy concerns as patients are live donors. However, all raw data used for this manuscript can be accessed by submitting a request to the sponsor at [studio.entire@ashermantherapy.com](mailto:studio.entire@ashermantherapy.com). A 36-month restriction applies, as required by the sponsor's intellectual property (IP) protection policy to safeguard ongoing clinical development and patent activities. All requests will undergo scientific and ethical review and sponsor's response will be provided within 30 days of receipt of a complete application.

### Code availability

All code used in this study is freely available online and can be found on <https://github.com/FCS-BioIT/asherman-trial-cd133-cell-therapy-public>

### REFERENCES

1. Dmowski, W. P. & Greenblatt, R. B. Asherman's syndrome and risk of placenta accreta. *Obstet Gynecol* **34**, 288-299 (1969).
2. Santamaria, X., Isaacson, K. & Simón, C. Asherman's Syndrome: it may not be all our fault. *Hum Reprod* **33**, 1374-1380 (2018).
3. Santamaria, X. et al. Decoding the endometrial niche of Asherman's Syndrome at single-cell resolution. *Nat Commun* **14**, 5890 (2023).

4. Hooker, A. B. et al. Systematic review and meta-analysis of intrauterine adhesions after miscarriage: prevalence, risk factors and long-term reproductive outcome. *Hum. Reprod. Update* **20**, 262-278 (2014).
5. Pabuccu, R. et al. Efficiency and pregnancy outcome of serial intrauterine device-guided hysteroscopic adhesiolysis of intrauterine synechiae. *Fertil Steril* **90**, 1973-1977 (2008).
6. Pistofidis, G. A., Dimitropoulos, K. & Mastrominas, M. Comparison of Operative and Fertility Outcome Between Groups of Women with Intrauterine Adhesions after Adhesiolysis. *J Am Assoc Gynecol Laparosc* **3**, S40 (1996).
7. Santamaria, X., Mas, A., Cervelló, I., Taylor, H. & Simon, C. Uterine stem cells: from basic research to advanced cell therapies. *Hum Reprod Update* **24**, 673-693 (2018).
8. Alawadhi, F., Du, H., Cakmak, H. & Taylor, H. S. Bone Marrow-Derived Stem Cell (BMDSC) transplantation improves fertility in a murine model of Asherman's syndrome. *PLoS One* **9**, e96662 (2014).
9. Cervello, I. et al. Human CD133(+) bone marrow-derived stem cells promote endometrial proliferation in a murine model of Asherman syndrome. *Fertil Steril* **104**, 1552-1553 (2015).
10. Santamaria, X. et al. Autologous cell therapy with CD133+ bone marrow-derived stem cells for refractory Asherman's syndrome and endometrial atrophy: a pilot cohort study. *Hum Reprod* **31**, 1087-1096 (2016).
11. (COMP), C. O. M. P. EMA/206895/2017. (2017).
12. The American Fertility Society classifications of adnexal adhesions, distal tubal occlusion, tubal occlusion secondary to tubal ligation, tubal pregnancies, mullerian anomalies and intrauterine adhesions. *Fertil Steril* **49**, 944-955 (1988).
13. Wyatt, K. M., Dimmock, P. W., Walker, T. J. & O'Brien, P. M. Determination of total menstrual blood loss. *Fertil Steril* **76**, 125-131 (2001).
14. Miller, T. E. et al. Mitochondrial variant enrichment from high-throughput single-cell RNA sequencing resolves clonal populations. *Nat Biotechnol* **40**, 1030-1034 (2022).
15. Xiao, S. et al. Etiology, treatment, and reproductive prognosis of women with moderate-to-severe intrauterine adhesions. *Int J Gynaecol Obstet* **125**, 121-124 (2014).
16. Yu, D., Wong, Y. M., Cheong, Y., Xia, E. & Li, T. C. Asherman syndrome-one century later. *Fertil Steril* **89**, 759-779 (2008).
17. Pittenger, M. F. et al. Multilineage Potential of Adult Human Mesenchymal Stem Cells. *Science* **143**, (2008).
18. Davies, L. C., Jenkins, S. J., Allen, J. E. & Taylor, P. R. Tissue-resident macrophages. *Nat Immunol* **14**, 986-995 (2013).
19. Li, Z. et al. Transplantation of human endometrial perivascular cells with elevated CYR61 expression induces angiogenesis and promotes repair of a full-thickness uterine injury in rat. *Stem Cell Res Ther* **10**, 179 (2019).
20. Slater, T., Haywood, N. J., Matthews, C., Cheema, H. & Wheatcroft, S. B. Insulin-like growth factor binding proteins and angiogenesis: from cancer to cardiovascular disease. *Cytokine Growth Factor Rev* **46**, 28-35 (2019).
21. Milingos, D. S. et al. Insulinlike growth factor-1Ec (MGF) expression in eutopic and ectopic endometrium: characterization of the MGF E-peptide actions in vitro. *Mol Med* **17**, 21-28 (2011).
22. Horikawa, S. et al. PDGFR $\alpha$  plays a crucial role in connective tissue remodeling. *Sci Rep* **5**, 1-14 (2015).

23. Balko, J. M. et al. The receptor tyrosine kinase ErbB3 maintains the balance between luminal and basal breast epithelium. *Proc Natl Acad Sci USA* **109**, 221-226 (2012).
24. Edeling, M., Ragi, G., Huang, S., Pavenstädt, H. & Susztak, K. Developmental signalling pathways in renal fibrosis: the roles of Notch, Wnt and Hedgehog. *Nat Rev Nephrol* **12**, 426-439 (2016).
25. Bachelier, K., Bergholz, C. & Friedrich, E. B. Differentiation potential and functional properties of a CD34-CD133+ subpopulation of endothelial progenitor cells. *Mol Med Rep* **21**, 501-507 (2020).
26. Díaz-Gimeno, P. et al. A genomic diagnostic tool for human endometrial receptivity based on the transcriptomic signature. *Fertil Steril* **95**, 50-60, 60.e1 (2011).
27. Moreno, I. et al. Evidence that the endometrial microbiota has an effect on implantation success or failure. *Am J Obstet Gynecol* **215**, 684-703 (2016).
28. SELDINGER, S. I. Catheter replacement of the needle in percutaneous arteriography; a new technique. *Acta Radiol (Stockh)* **39**, 368-376 (1953).
29. Bankhead, P. et al. QuPath: Open source software for digital pathology image analysis. *Sci Rep* **7**, 16878 (2017).
30. Chen, S., Zhou, Y., Chen, Y. & Gu, J. fastp: an ultra-fast all-in-one FASTQ preprocessor. *Bioinformatics* **34**, i884-i890 (2018).
31. Danecek, P. et al. Twelve years of SAMtools and BCFtools. *Gigascience* **10**, giab008 (2021).
32. Quinlan, A. R. & Hall, I. M. BEDTools: a flexible suite of utilities for comparing genomic features. *Bioinformatics* **26**, 841-842 (2010).
33. Wilm, A. et al. LoFreq: a sequence-quality aware, ultra-sensitive variant caller for uncovering cell-population heterogeneity from high-throughput sequencing datasets. *Nucleic Acids Res* **40**, 11189-11201 (2012).
34. DePristo, M. A. et al. A framework for variation discovery and genotyping using next-generation DNA sequencing data. *Nat Genet* **43**, 491-498 (2011).
35. Robinson, J. T. et al. Integrative genomics viewer. *Nat Biotechnol* **29**, 24-26 (2011).
36. Hao, Y. et al. Dictionary learning for integrative, multimodal and scalable single-cell analysis. *Nat Biotechnol* **42**, 293-304 (2024).
37. Borchering, N. et al. Mapping the immune environment in clear cell renal carcinoma by single-cell genomics. *Commun. Biol* **4**, 1-11 (2021).
38. Wang, W. et al. Single-cell transcriptomic atlas of the human endometrium during the menstrual cycle. *Nat Med* **26**, 1644-1653 (2020).
39. Boretto, M. et al. Development of organoids from mouse and human endometrium showing endometrial epithelium physiology and long-term expandability. *Development* **144**, 1775-1786 (2017).
40. Boretto, M. et al. Patient-derived organoids from endometrial disease capture clinical heterogeneity and are amenable to drug screening. *Nat Cell Biol* **21**, 1041-1051 (2019).
41. European IVF-Monitoring Consortium (EIM) for the European Society of Human Reproduction and Embryology, E. S. H. R. E. et al. Assisted reproductive technology in Europe, 2012: results generated from European registers by ESHRE. *Hum Reprod* **31**, 1638-1652 (2016).

### Acknowledgments

We thank the patients who participated in this trial and their families, the investigators, staff at the clinical sites, and the members of the independent data and safety monitoring committee. We also thank Hilary Critchley (University of Edinburgh) for critical assessment and editing of the manuscript. Samsung (Seoul, South Korea) for supporting the trial providing appropriate software for the 3D ultrasound analysis. We would also like to thank Adrián Gonzalez for support in figure design, to R. Pérez-Moraga for his valuable bioinformatic support and Ana Monteagudo for her help in setting up the MAESTER technique. We vouch for the accuracy and completeness of the data and analysis, as well as the adherence of the study to the protocol and statistical analysis plan, which are available upon request at estudio.entire@ashermantherapy.com.

### Authors Contribution Statement

XS and CS conceptualized and designed the study. XS supervised the study, acquired and interpreted the data. XS, MPF, JGF, CG and EF collaborated in collecting the data and drafting of figures and tables to report the data. SQ, LR, DV, CG, EF, MR, RA, CG and JT collected data. SG and RN contributed to digital microscopic analysis. DA and PV performed the scRNA-seq analysis. MR, MPF, CG and DVB contributed to statistical analysis. SZ and FM completed the lineage tracing analysis. CS, MPF and XS drafted the manuscript. JGF, SQ, DV, CG, LR, RA, JT, HT, FV, FR and JH critically reviewed the work. XS, MPF, JGF and CS accessed and verified the data in the study. All authors had full access to all the data and had final responsibility for the decision to submit for publication.

### Competing Interest Statement

C.S. & X.S. are founders, shareholders of Asherman Therapy S.L. and inventors of patents granted in Europe, Australia, Canada, Japan, Russian Federation, Mexico, and the US derived from PCT application PCT/IB2015/001715. MPF and EF are employees of Asherman Therapy SL. MPF has been awarded a Torres Quevedo Grant (PTQ2022-012376). CS has received consulting fees from Vitrolife. RA, SQ, CG, JT and JH have no potential conflict of interest with this therapy nor

Asherman Therapy SL. DV has received consulting fees, honoraria for lectures or educational events from Amgen, BMS/Celgene, Kite/Gilead, Novartis, Sanofi, Grifols, Jad Pharmaceuticals, MDS, Pfizer, Sobe, Astellas, Jansen and Gebro. SG is employed by Ciberonc (CB16/12/00484). This study was also partially supported by research grants PROMETEO/2018/161 from the Valencia Government, IDI-20201142 CDTI from the Centro Desarrollo Tecnológico e Industrial (CDTI, Spain) and the KY Cha Award for Stem Cell Technologies of the American Society of Reproductive Medicine (ASRM) and was partly supported by FIS (Institute of Health Carlos III, Madrid/ERDF, PI20/01107) and CIBERONC (CB16/12/00484).

## Legends

### Table Legends

**Table 1. Patient metadata.** Pre-treatment and post-treatment assessment (2D/3D vaginal ultrasound, hysteroscopic scores) one month after cell therapy. Reproductive function assessment after single embryo transfer post cell therapy. One patient did not complete the study.

**Table 2. Summary of adverse events (AEs) after stem cell administration.**

**Table 3. Pictorial Blood Assessment Chart (PBAC Scoring).**

**Figure 1. Clinical workflow of AS therapy.** A) The timing of assessments and B) Trial profile.

**Figure 2. Effect of CD133+ therapy on the endometrium.** A) Effect of the autologous CD133+ BMDSC therapy on the endometrial thickness and volume assessed by 2D and 3D vaginal ultrasound pre- (Pre-AS therapy) and one-month post-therapy (Post-AS therapy). Data shown are from the 16 patients with both 2D and 3D endometrial measurements available. B) Box plots of endometrial thickness (n=19), and (C) endometrial volume (n=16) of AS patients pre- and post-AS therapy representing all data before and after one month of cell therapy. Endometrial volume data for three patients (n=16/19) could not be measured due to unavailability of the 3D transvaginal probe at the time of patient follow-up. Whisker ends on the box plot represent the minimum and the maximum data point. Two-sided paired t-test; \*\*\*\* p<0.0001.

**Figure 3. Effect of CD133+ therapy in the endometrial cavity.** A) Representative hysteroscopic images of the effect of the autologous CD133+ BMDSC therapy on the endometrial cavity assessed by hysteroscopic scores performed pre (Pre-AS therapy), and one-month post-therapy (Post-AS therapy) according to the IUA ASRM score. Representative hysteroscopy images of the four remaining patients (n=15/19) could not be illustrated due to technical limitations of hysteroscopy equipment at the time of patient follow-up. Hysteroscopic images consistently show constricted uterine cavities by IUAs with limited space pre-AS therapy while images demonstrate a significantly widened uterine cavity, indicating successful structural remodeling post-AS therapy. B) Box plots of IUAs score from AS patients (n=19) pre-AS therapy (8±3.17) and post-AS therapy (4.42±2.09). Whisker ends on the box plot represent the minimum and the maximum data point. Wilcoxon test; \*\*\*\* p<0.0001.

**Figure 4. Transcriptomic analysis in AS patients pre- and post-AS therapy.** A) UMAP of scRNA-seq results from nine AS patients before (Pre-AS therapy, n=40,336 cells) and after therapy (Post-AS therapy, n=82,914 cells). B) Boxplot of enrichment score results (UCellScore) of gene signature characteristic of the secretory phase in the menstrual cycle. C) Box plots of cell type ratios comparing pre- and post-AS therapy (NB-GLM statistical test\*\* = FDR<0.05, \*= FDR<0.1). D) Relative and absolute information flows of each signaling pathway differentially detected in AS patients pre- and post-AS therapy (Wilcoxon; FDR <0.05). E) UMAPs of three AS patients (33,464 cells) post-AS therapy annotated by transcriptional signatures (above) and selected mtDNA clones (below).

**Figure 5. *In vitro* model of epithelial endometrial organoids pre- and post-AS therapy.** A) Images of organoid culture generated from patient's pre- and post-AS therapy at different passages (P0= Passage 0, P1= Passage 1, P2= Passage 2) and controls, as well as the number of organoids counted in different passages (n=3). Differences between groups were analyzed using the Tukey's multiple comparison test (\*\*p<0.01, \*p<0.05). B) UMAP of scRNA-seq results of main cell types identified in endometrial epithelial organoids from healthy control samples (Control EEO, 15,594 cells), Pre-AS therapy (AS EEO, 14,459 cells), and Post-AS therapy (AS-Post EEO, 19,556 cells).

C) Cell type proportion across pre-AS therapy (Pre-AS EEOs), post-AS therapy (Post-AS therapy) and Control (Control EEO) endometrial epithelial organoids.

**Table 1.** Patient metadata. Pre-treatment and post-treatment assessment (2D/3D vaginal ultrasound, hysteroscopic scores) one month after cell therapy. Reproductive function assessment after single embryo transfer post cell therapy. One patient did not complete the study.

Grade of AS	Previous pregnancies prior to AS diagnosis	Previous miscarriages prior to AS	Live birth prior to AS diagnosis	Dosage ( $10^6$ CD133+ cells)	3D Endometrial Volume ( $cm^3$ ) post	Pregnancies post-therapy	Outcomes
Severe	Yes	No	Yes	165.8	2.43	Yes	Biochemical (1) Non pregnancy (2)
Severe	Yes	No	Yes	51.8	0.48	No	Non pregnancy (1)
Moderate	Yes	Yes	No	120.0	2.23	No	Non pregnancy (2)
Severe	Yes	No	Yes	136.0	1.71	No	Non pregnancy (1)
Severe	Yes	Yes	No	131.0	2.43	No	Non pregnancy (1)
Severe	No	No	No	123.0	2.95	No	Non pregnancy (2)
Moderate	Yes	Yes	No	155.0	3.88	Yes	Biochemical (1)+ live birth (1)
Moderate	Yes	Yes	No	170.0	4.18	Yes	Clinical miscarriage (1) Non pregnancy (2)
Moderate	Yes	Yes	No	31.0	2.91	Yes	Biochemical (1) + live birth (1)
Severe	Yes	No	Yes	85.3	1.63	No	Non pregnancy (2)
Moderate	Yes	Yes	Yes	96.4	**	Yes	Live birth
Moderate	Yes	Yes	No	159.0	N/A	No	Non pregnancy (2)
Moderate	Yes	Yes	No	40.5	N/A	Yes	Biochemical (1) Non pregnancy (1)

Moderate	Yes	Yes	No	167.0	N/A	No	Biochemical (1) Non pregnancy (2)
Moderate	Yes	Yes	Yes	80.6	3.53	Yes	Live birth (1) Non pregnancy (1)
Moderate	Yes	No	Yes	153.0	2.47	Yes	Clinical (1) Non pregnancy (1)
Moderate	Yes	Yes	Yes	212.0	4.93	Yes	Live birth (1) Non pregnancy (3)
Severe	No	Yes	No	111.0	4.18	No	Non pregnancy (1)
Severe	Yes	No	Yes	147.0	1.75	No	Non pregnancy (3)
Moderate	Yes	No	Yes	102.0	2.83	Yes	Live birth (1) + biochemical (1) + Non pregnancy (1)

**Table 2.** Summary of adverse events (AEs) after stem cell administration.

Adverse events	Number of affected patients	Percentage affected patients (%, n=20)
<b>GYNECOLOGICAL SYMPTOMS</b>		
None	13	65
Uterine pain	3	15
False passage after hysteroscopy	2	10
Ovarian pain	1	5
Right breast pain	1	5
Dizziness (due to menstrual metrorrhagia)	1	5
Vaginal infection	1	5
Vaginal itching	1	5
Ovarian cyst	1	5
Vaginal Bleeding	1	5
Bilateral galactorrhea	1	5
Unilateral galactorrhea	1	5
<b>DIGESTIVE SYMPTOMS</b>		
None	12	60
Nausea	4	20
Abdominal pain	3	15
Diarrhea	2	10
Throat pain	2	10
Weight gain	1	5
Abdominal pain with nausea	1	5
Hemorrhoid pain	1	5

Vomiting	1	5
Bloating	1	5
<b>CARDIOVASCULAR SYMPTOMS</b>		
None	15	75
Hematoma in arm	2	10

Pain associated with arm hematoma	1	5
Superficial thrombophlebitis in right leg	1	5
Vasospasm in right uterine artery	1	5
<b>GENERAL SYMPTOMS</b>		
None	18	90
Cramps	2	10
Generalized pain	1	5
Fatigue	1	5
<b>DERMATOLOGICAL SYMPTOMS</b>		
None	17	85
Facial erythema	2	10
Eczema in abdominal area	1	5
Neck erythema	1	5
Catheter arm rash	1	5
Localized skin rash	1	5
<b>MUSCULO-SKELETAL SYMPTOMS</b>		
None	12	60
Arm pain	4	20
Neck pain	2	10
Low back pain /Lumbago	2	10
Spasm caused by the introducer in left arm	1	5
Chest pain	1	5
Back pain	1	5
Finger pain	1	5
Toe pain	1	5
Foot pain	1	5
Left leg pain	1	5
<b>NEUROLOGICAL SYMPTOMS</b>		
None	12	60
Headache	8	40

Paresthesia in hands and feet	1	5
Paresthesia in lips and hands	1	5
Feeling of nervousness around the heart	1	5
<b>RESPIRATORY SYMPTOMS</b>		
None	19	95
Asthma	3	15
Upper respiratory infection	1	5

**Table 3.** Pictorial Blood Assessment Chart (PBAC Scoring).

\* Patient did not complete the protocol.

\*\*Patient did not have MP

\*\*\*Patient did not complete the requested information

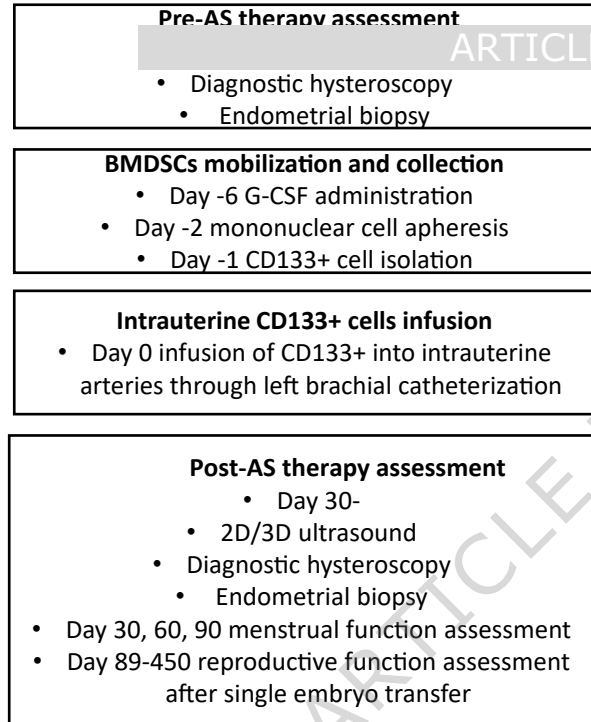
ID	MP 1	MP 2	MP 3	MP 4	MP 5	MP 6
N1	11	22	8	***	***	***
N2	***	**	***	***	***	***
N3	11	13	**	**	***	***
N4	9	440	260	0	420	50
N5	20	32	68	109	***	***
N6	52	60	14	55	32	20
N7	14	18	24	42	36	
N8	14	34	9	**	***	***
N9	181	38	5	**	9	11
N10	2	0	2	7	2	12
N11	*	*	*	*	*	*
N12	***	***	***	***	***	***
N13	6	39	56	42	52	68
N14	6	49	61	28	48	17
N15	28	28	35	38	37	**
N16	***	***	***	***	***	***
N17	***	***	***	***	***	***
N18	62	51	44	24	22	35
N19	13	24	14	17	20	24
N20	26	2	8	12	12	12

MP =Menstrual Period

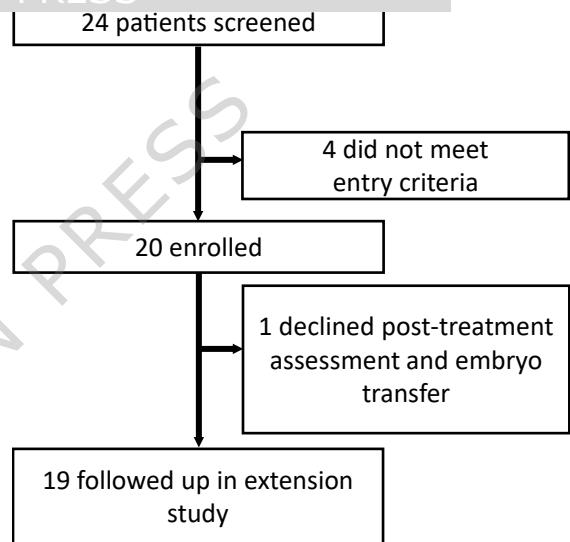
**Editorial Summary**

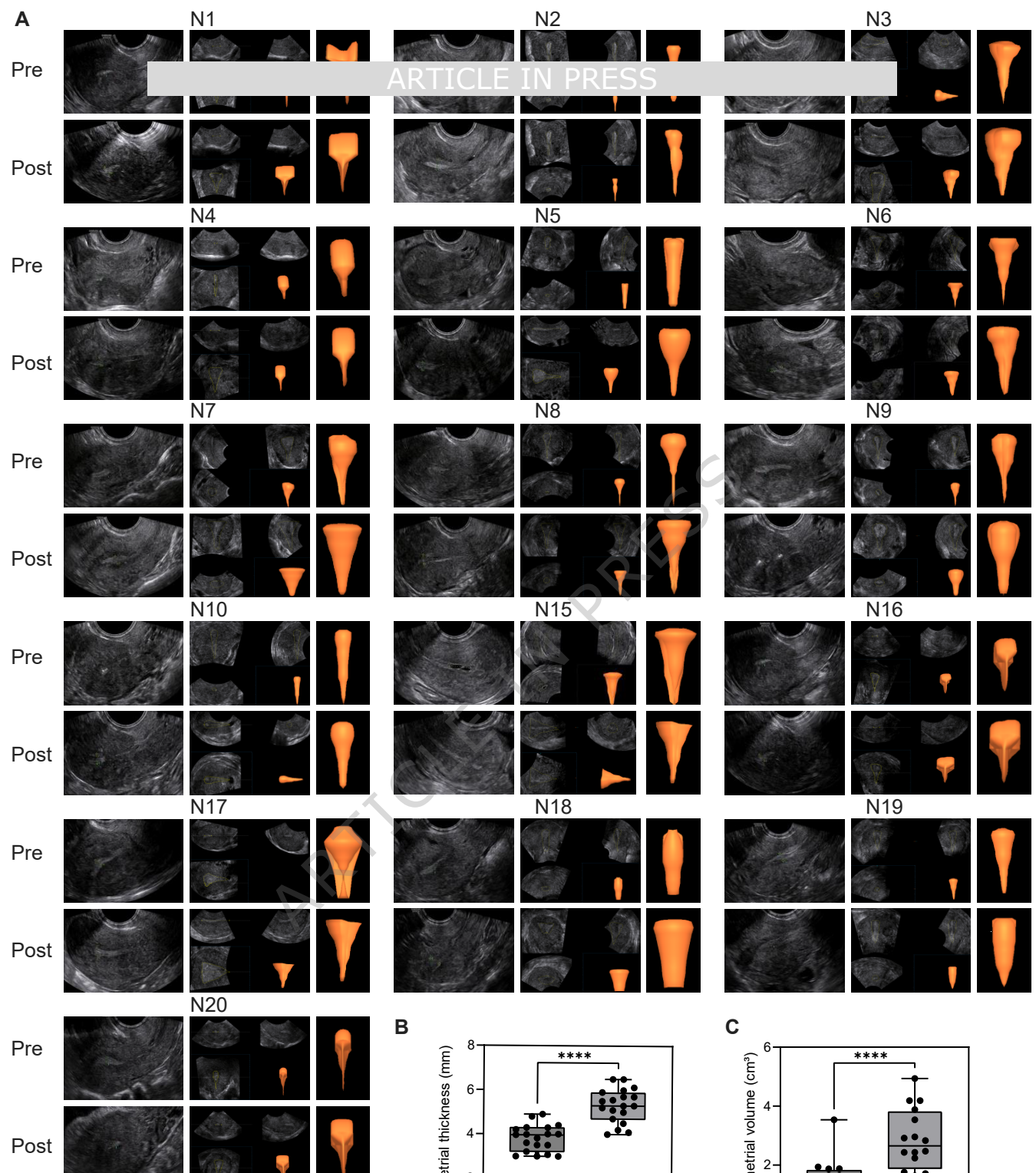
The authors present the results of a phase I/II clinical trial using autologous CD133+ bone marrow stem cell therapy to restore fertility in patients with Asherman Syndrome. The intervention was safe and showed promising results for the restoration of menstruation and reproductive function.

**Peer Review Information:** *Nature Communications* thanks Lusine Aghajanova , Markus Wolfien, Yali Hu and Leonardo Emberti Gialloreti who co-reviewed with Mariagrazia Cicala and the other anonymous, reviewer(s) for their contribution to the peer review of this work. A peer review file is available.

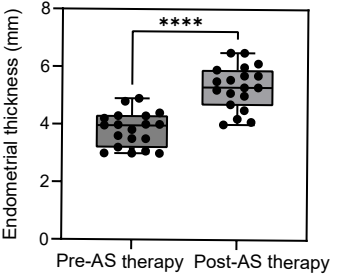


## ARTICLE IN PRESS

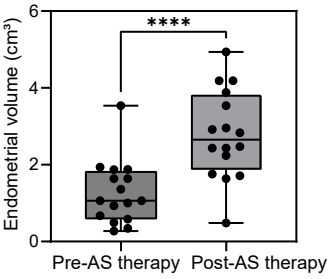


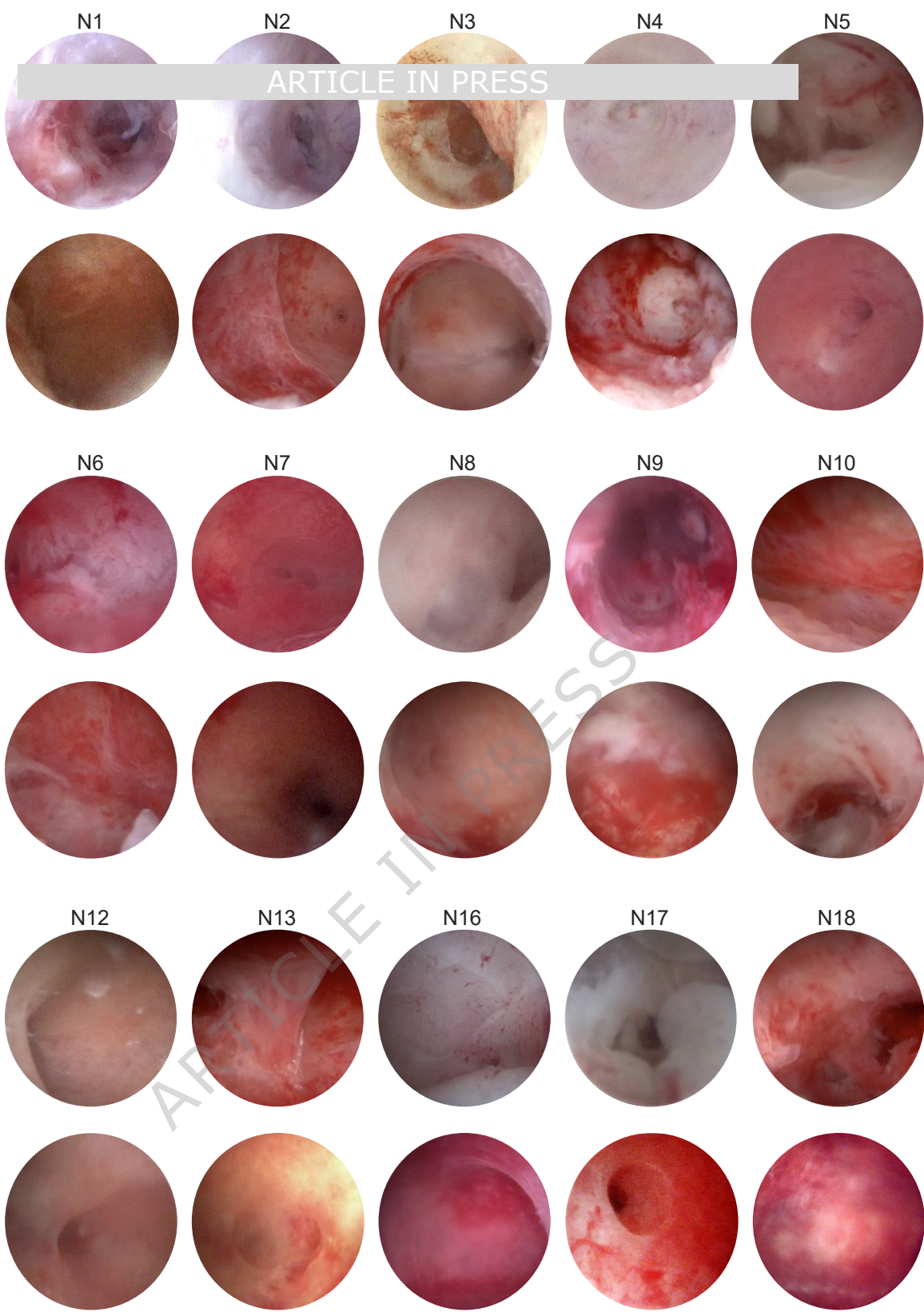
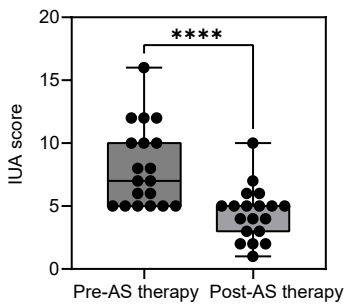


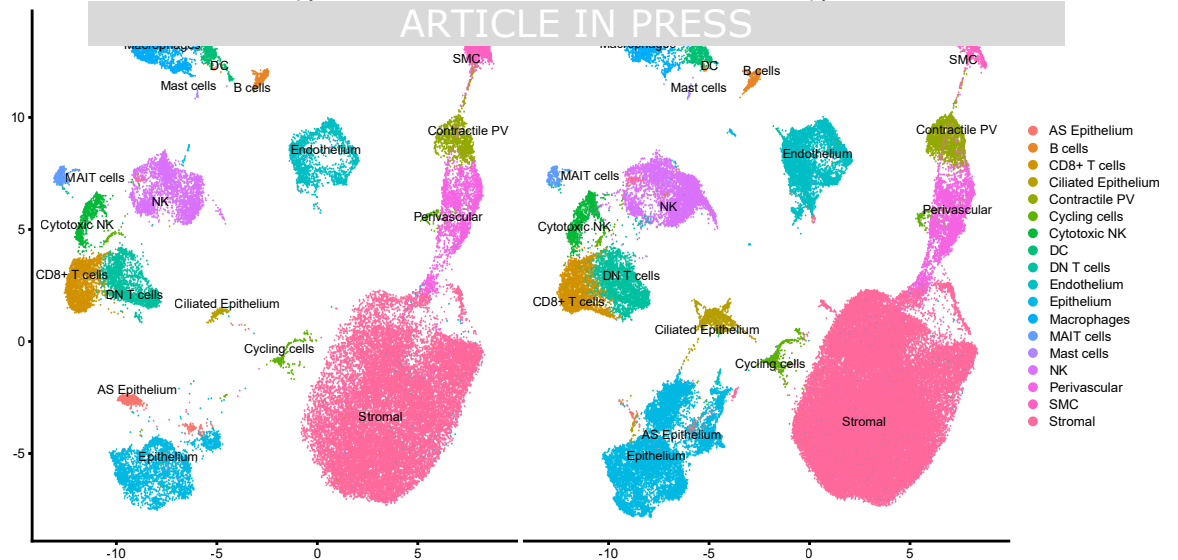
**B**



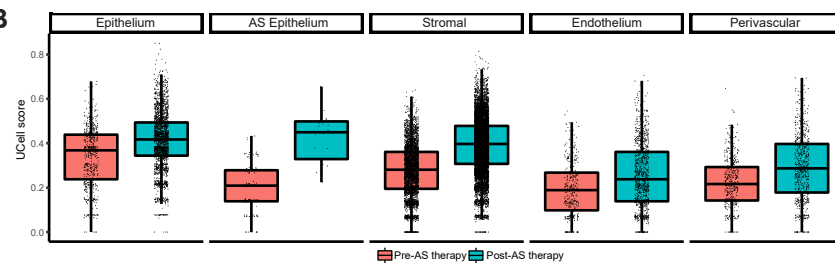
**C**



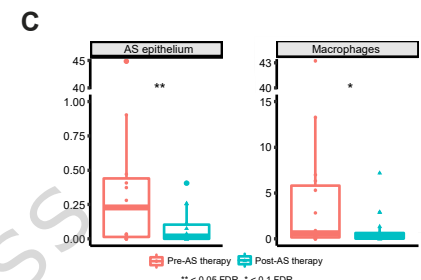
**A****B**



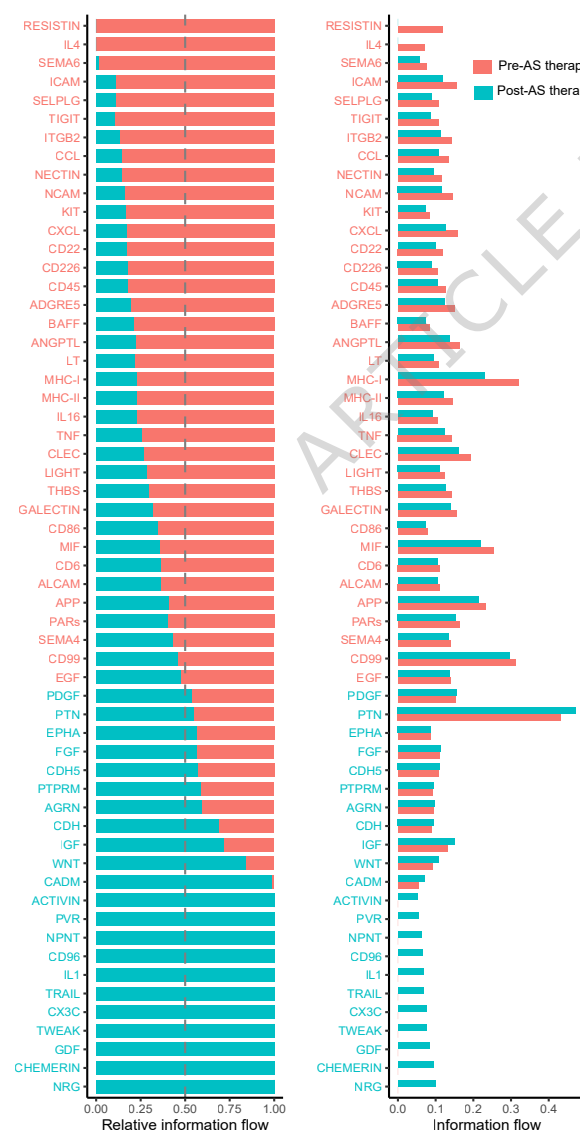
B



C



D



E

